

Quantum efficiency of III-Nitride emitters: evidence for defect-assisted non-radiative recombination and its effect on the green gap

Aurelien David,* Nathan G. Young, Christophe A. Hurni, and Michael D. Craven
Soraa Inc., 6500 Kaiser Dr. Fremont CA 94555
 (Dated: December 15, 2024)

Carrier lifetime measurements reveal that, contrary to common expectations, the high-current non-radiative recombination (droop) in III-Nitride light emitters is comprised of two contributions which scale with the cube of the carrier density: an intrinsic recombination –most likely standard Auger scattering– and an extrinsic recombination which is proportional to the density of point defects. This second droop mechanism, which hasn't previously been observed, is likely caused by an impurity-assisted Auger process. Further, it is shown that longer-wavelength emitters suffer from higher point defect recombinations, in turn causing an increase in the extrinsic droop process. It is proposed that this effect leads to the green gap, and that point defect reduction is a strategy to both vanquish the green gap and more generally improve quantum efficiency at high current.

Although modern III-Nitride light-emitting diodes (LEDs) can reach very high efficiency [1], they still suffer from two important limitations. First, their internal quantum efficiency (IQE) decreases at high current, an effect known as efficiency droop. It is by now generally believed that droop is, at least in part, caused by Auger scattering – owing to the approximately-cubic dependence of the droop current on carrier density [2, 3], and the observation of Auger electrons [4]. Second, IQE decreases at long wavelength (corresponding to a high In content in the active region), a phenomenon of controversial origin known as the green gap. Various explanations have been offered for the green gap. It has been proposed that high-In quantum wells (QWs) suffer from an increase in point defects [5, 6] – however this should only impact low-current recombinations, whereas the green gap occurs at all currents. Other tentative explanations include an increase in electron-hole separation (leading to weaker radiative recombinations), due to increasing polarization fields and in-plane carrier localization [7–9]. Crucially, these explanations don't clarify the role played by non-radiative recombinations in the green gap. The combined effects of droop and the green gap have made it challenging to achieve efficient long-wavelength LEDs at high current density.

In this Letter, we show that these two phenomena are connected and propose a mechanism for the green gap. We investigate droop dynamics in greater detail, and show that droop is in fact caused by a combination of two processes – one intrinsic, the other extrinsic and scaling with point defect concentration. We then confirm that high In content leads to an increase in point defect recombinations, which in turn leads to an increase of the extrinsic droop component and the appearance of the green gap.

We study samples with 4 nm-thick single-QWs within p-i-n regions, grown on c-plane bulk GaN substrates by MOCVD; these samples include an InGaN underlayer (UL) beneath the p-i-n region, which improves material quality [10–12]. Importantly, the QW is placed at the

center of the intrinsic region to avoid modulation-doping, which would alter the recombination dynamics.[13]

We first summarize important properties of the recombination dynamics in InGaN QWs. We measure carrier lifetimes (τ) with an optical differential lifetime (ODL) technique under laser excitation, whose details are found in Ref. [14]. ODL uniquely enables the measurement of lifetimes down to low current density –in the Shockley-Read-Hall (SRH) regime– and is devoid of electrical injection artifacts [15]. We obtain τ as a function of the optical current density (J) in the QW, and concurrently measure the sample's absolute IQE. This yields the carrier density (n) in the QW and the radiative and non-radiative rates (G_R , G_{NR}), from which we derive three important quantities:

$$a = G_{NR}/n, \quad b = G_R/n^2, \quad c = (G_{NR} - An)/n^3. \quad (1)$$

These quantities assume a simple interpretation in the framework of the well-known *ABC* model: at low current, a should be equal to the SRH coefficient A ; while at all currents, b and c should be constant, and respectively equal to the radiative coefficient B and the Auger coefficient C . For now, we place ourselves in this framework – although the interpretation of c will be refined hereafter. In practice A is first extracted from the low-current plateau of a , and this value is then subtracted in Eq. 1 to calculate c .

Experiments have shown that b and c are in fact current-dependent quantities [14]. As shown in Fig. 1 (for a sample with [In]=13%), they increase with carrier density due to screening of the polarization field across the QW – which induces an increase of the electron-hole overlap $I = \int \psi_e \psi_h$. It is well-known that $B \sim I^2$ [16]. Regarding Auger scattering, experiments and calculations have shown that $C \sim I^p$, with $p \approx 2 - 3$ (depending on the mixture of *eeh* and *ehh* contributions) [14, 17, 18].

I can be decomposed according to $I(n) = I_0 S(n)$, where I_0 is the low-current value of I and S a screening

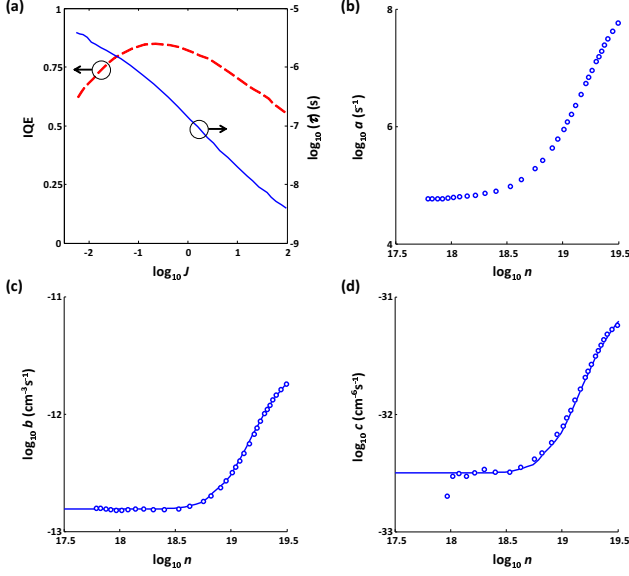


FIG. 1. Results from ODL measurements of a single-QW sample. (a) Lifetime (full line) and IQE (dashed line). (b) Non-radiative component a , whose low-current plateau gives the SRH coefficient A . (c) Radiative component b showing the carrier-dependence of radiative recombinations. Symbols: experimental data; line: empirical fit of the data, from which the screening function S is derived (i.e. $b \sim S^2$). (d) Non-radiative component c showing the carrier-dependence of Auger scattering. Symbols: experimental data; line: fit by $c \sim S^p$.

function accounting for the effect of carriers on the potential, with S normalized to unity at low current. Often S is evaluated numerically from a simple one-dimensional Poisson-Schrodinger model, as was done in Ref. [14] – however, such computations are of limited accuracy as they ignore in-plane carrier localization. Instead, in this Letter, we derive S empirically from $S = \sqrt{b/B_0}$. The overlap dependence of C can then be explicitly verified, as shown on Fig. 1(d): we find that $p \approx 2.4$, indicating a mixture of eeh and ehh Auger processes. Thus, we have $b = B_0 S^2$ and $c = C_0 S^p$, with the low-current values (subscript 0) obtained before the onset of screening.

Further, we showed in Ref. [19] that the coefficient A , derived from Eq. 1, also scales with wavefunction overlap. Indeed, both electrons and holes need to be present at a point defect to complete a SRH recombination cycle. Experimentally, we find $A \sim I^q$ with $q \approx 1.6$. [20]

In summary, all three recombination mechanisms scale with similar exponents of the overlap I . Thus, for various active regions spanning a large range of overlaps, these dependencies cancel out, leading to nearly-constant peak IQE, as shown in Ref. [19].

Given this backdrop, we now study a series of samples where the SRH rate is intentionally varied by one of three methods. In a first case, we vary the epi growth between conditions labeled 1 and 2 (with 2 being comparatively

TABLE I. Sample details (UL refers to the relative thickness of the UL layer, values of A and c_0 are in \log_{10} scale).

#	growth	UL	ΔT	$A(s^{-1})$	$c_0(cm^{-6}s^{-1})$
1	1	100%	0	4.78	-32.49
2	2	100%	0	5.44	-32.10
3	2	80%	0	5.67	-31.96
4	2	50%	0	6.38	-31.33
5	2	20%	0	6.72	-31.07
6	2	0%	0	7.21	-30.79
7	2	100%	+150C	6.41	-31.33

worse); in a second case, we vary the UL thickness (with a thinner UL leading to lower IQE); in a third case, we increase by ΔT the growth temperature of the intrinsic GaN layer underneath the QW [21] (leading to lower IQE). Importantly, in all samples, the active region is identical, with $[In] = 13\%$. Table I shows the details of the samples. Fig. 2 shows each sample's IQE and quantities (b , c) determined from ODL measurements. Quantity a (not shown) displays a clear low-current plateau for each sample, from which A is extracted.

IQE varies significantly across the series. The samples with higher A suffer from low IQE at low current, as expected. However, their high-current IQE is also impacted. This is surprising because SRH recombinations should have little influence beyond $\sim 100A.cm^{-2}$. To illustrate this, we model the expected impact of increasing A while b and c remain unchanged for each sample (with values of b , c taken from the brightest sample). Fig. 2(a) shows all modeled curves converging at high J , in contrast to the data. To explain this discrepancy, we turn our attention to the other recombination channels.

Fig. 2(b) shows that b is near-identical for all samples, indicating the radiative rate is the same, as expected since they have the same active region. Incidentally, this confirms the accuracy of the ODL technique for measuring recombination rates, since all samples have markedly different lifetimes and IQEs, but the same b is derived from each.

In contrast, in Fig. 2(c), c shows a strong variation (more than one order of magnitude) across the series: the samples with higher A also have higher c . This is unexpected if we simply attribute C to Auger scattering – an intrinsic process, which should be constant for all samples just like radiative recombination. Instead, the interpretation of c has to be revised; the data lends itself to the following decomposition:

$$c = C_0 S^p n^3 + D n^3, \quad (2)$$

where C_0 is an intrinsic Auger coefficient (constant for all samples) and D denotes a second, extrinsic droop process which scales with A . This decomposition yields good

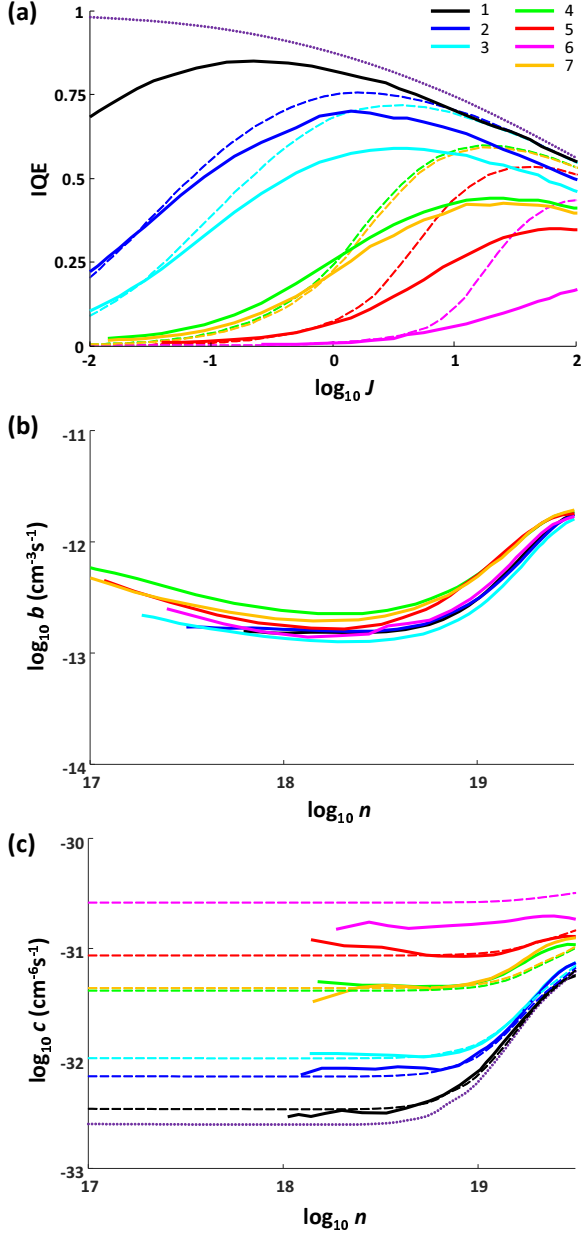


FIG. 2. ODL-derived results of Table I samples. (a) Full lines: experimental IQE. Dashed lines: modeled IQE for varying A but constant values of b and c ; the model doesn't predict the decrease in IQE at high current. Dotted line: theoretical IQE limit in the intrinsic case ($A = 0$, $D = 0$). (b) The radiative term b is nearly-identical for all samples. (c) The non-radiative term c (full lines) varies across the series. Dashed lines: fits according to Eq. 2. Dotted line: intrinsic Auger component, resulting in the dotted line in (a).

fits for values of C_0 in the range $2\text{--}3\text{E-}33 \text{ cm}^{-6}\text{s}^{-1}$. Hereafter, we use $C_0 = 2.5\text{E-}33 \text{ cm}^{-6}\text{s}^{-1}$, which leads to a close match to experimental data (shown in Fig. 2(c)), from which we derive the value of D for each sample.

Fig. 3 shows the resulting correlation between A and

D . The two coefficients are correlated with a slope in log-log scale of about unity (the precise value depends on the assumed value of C_0 , but remains in the range 0.8-1.2). We conclude that to first order $D = k \cdot A$ with $k = 2\text{E-}38 \text{ cm}^{-6}$, which we interpret as follows. For a given active region design, A is proportional to the concentration of a point defect causing SRH recombinations; our finding indicates that this same point defect also induces an Auger-like non-radiative process, which adds to the intrinsic Auger scattering present in all samples. Only for sample 1, which has the lowest defect density, is the droop near the intrinsic limit indicated in Fig. 2. Crucially, this shows that defect reduction is essential for high-current performance.

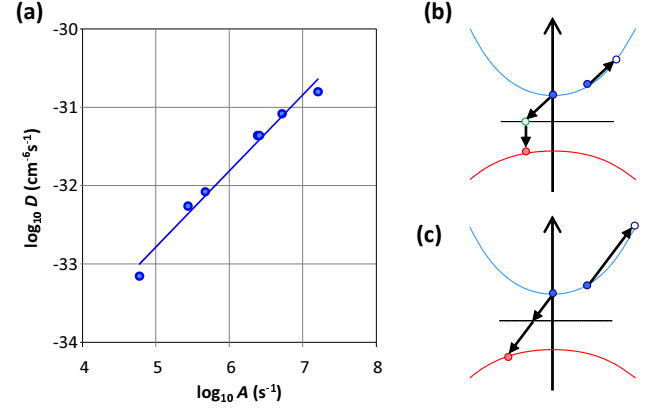


FIG. 3. (a) Correlation between the SRH coefficient A and the extrinsic droop coefficient D (in log-log scale), with a slope of 1 ± 0.2 . (b, c) Possible high-order processes involving a trap: (b) electron Auger scattering into a trap followed by SRH hole recombination with the trap; (c) eeh Auger process where the trap level acts as a virtual state.

Various high-order non-radiative mechanisms involving traps might be considered to account for the extrinsic process, as illustrated in Fig. 3(b-c). However, its well-defined cubic dependence on the carrier density (manifested as clear plateaus in Fig. 2(c)) imposes restrictions. Fig. 3(b) shows a combination of an Auger scattering to a trap state [22] followed by an SRH recombination; it can be verified that such processes have a carrier dependence in-between n and n^2 . More generally, processes generating a population in the trap state will deviate from an n^3 scaling. Therefore, we propose that the mechanism at play may instead be of the form shown in Fig. 3(c): Auger scattering involving the trap level as a virtual state, without population buildup. Further theoretical exploration would be warranted to determine if such processes are indeed likely in III-Nitrides.

To explore the broader implications of this extrinsic droop process, we now consider samples of varying QW composition in the range $[\text{In}] = 8\text{--}25\%$ – i.e. spanning the violet-to-green range.[23] We grow series of such samples

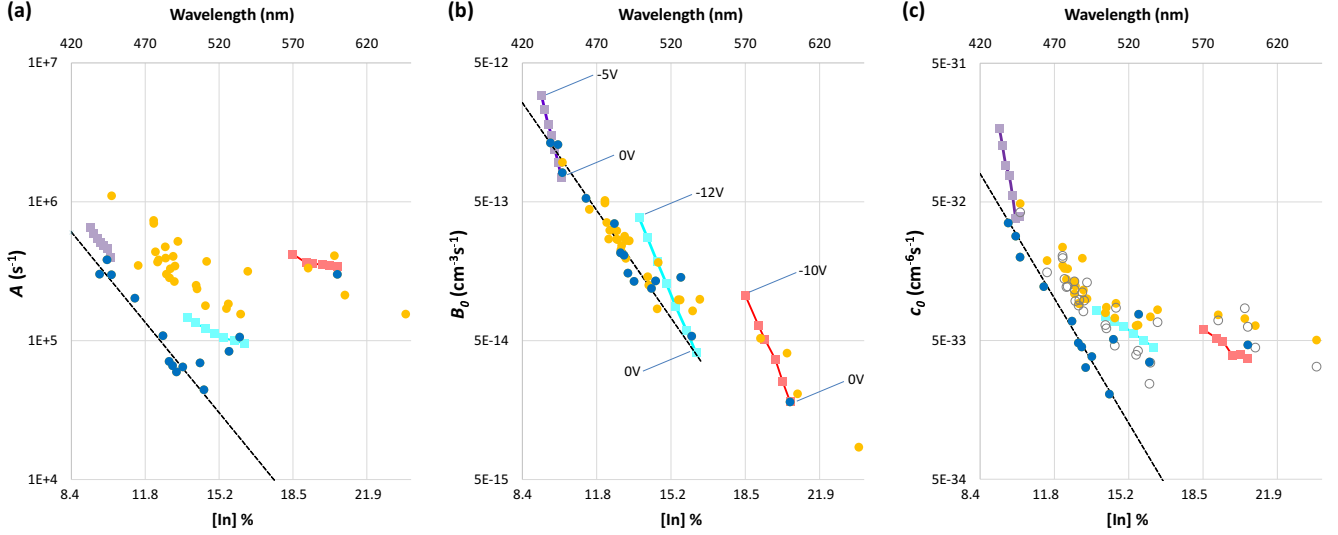


FIG. 4. (a-c) Recombination coefficients A , B_0 and c_0 , plotted as a function of emission wavelength and corresponding [In]. Symbols represent the following. Full dots: Samples of varying composition (blue dots: epi condition 1; yellow dots: epi condition 2). Open dots: predicted value of c_0 according to Eq. 2 (for samples with epi condition 2). Dashed lines: empirical wavefunction dependences $A \sim I^q$ ($q = 1.6$), $B \sim I^2$ and $C \sim I^p$ ($p = 2.3$). Full lines with squares: samples under reverse bias (purple/cyan/red: [In]=10%/16%/22% respectively). The bias endpoints are indicated on (b).

using epi conditions 1 and 2 mentioned above (and a full UL thickness of 100%). The study comprises 44 samples, whose values of A , B_0 and $c_0 = C_0 + D$ are measured by ODL and shown in Fig. 4. Their peak IQE is roughly constant in the violet-blue range (for a given epi condition) but decreases at longer wavelength – a manifestation of the green gap. The radiative rate is well-behaved, with Fig. 4(b) showing that B_0 decreases with higher [In] – as anticipated due to the decreasing wavefunction overlap and regardless of the epi growth condition.

Next we consider A (Fig. 4(a)) – which we expect to scale both with defect density and wavefunction overlap. Indeed, for moderate QW compositions ([In]= 8 – 15%), A decreases with [In] – the trend is clearest in samples with epi condition 1, but is also observed with condition 2 (albeit with higher values of A and more variability). This corresponds to the aforementioned regime, where the point defect incorporation remains constant and variations in A are driven by wavefunction overlap (i.e. $A \sim I^q$). However, for higher [In], this trend breaks down and A remains roughly constant as the QW composition increases. This marks a departure from the previous regime, and indicates that either (i) the point defect density increases with [In] and/or (ii) the overlap dependence of A is altered.

Remarkably, the trend for the droop coefficient $c_0 = C_0 + D$ closely follows that of A . For a given growth condition, c_0 first decreases with overlap before reaching an approximate plateau. We propose that the departure of c_0 from the intrinsic regime I^p is driven by variations in point defects, and hence D . To verify this, we show

in Fig. 4(c) the values of c_0 predicted by Eq. 2 – these closely match the experiment, confirming a systematic coupling between SRH defects and the extrinsic droop process.

To further understand the behavior of A and c_0 , we perform additional ODL measurements with a reverse bias applied to the samples. The reverse bias reduces the electric field across the QW [24] and the resulting quantum-confined Stark effect, enabling a direct measurement of the overlap-dependence of recombinations in a given sample. We measure three samples with [In]=10%, 16%, 22% (note that a reverse-bias photocarrier leakage current is observed for the 10% sample [25]; this effect is corrected-for in the data analysis). The results are included in Fig. 4, using the samples' wavelength to superimpose the data with the previous experiment. The bias-induced increase in overlap leads to a well-behaved increase in B_0 for all samples (the wavelength-dependence of these curves is slightly different from that of the previous experiment: this is because it is induced by a change in field, rather than composition). In contrast, the overlap-dependence of A is most pronounced for the low-content sample and nearly nonexistent for the high-content sample. Accordingly, c_0 shows a similar behavior.

Thus, as the QW's indium content increases, there is a transition from a “well-behaved” regime where all recombinations have pronounced overlap dependence (following the dashed lines in Fig. 4), to the green gap regime where A and c_0 become nearly constant (overlap-independent). This transition might be due to the formation of a differ-

ent SRH-causing defect, or to a change in the physics governing SRH recombinations in high-composition QWs.

In summary, we have shown two crucial results for understanding the efficiency of III-Nitride LEDs. First, droop has two contributions. In addition to the known intrinsic Auger scattering in low-defect materials, SRH-causing defects also induce an additional, extrinsic Auger-like non-radiative process which dominates droop in high-defect materials – in stark contrast with the common expectation that droop and defects are independent. Second, in long-wavelength samples with high In content, SRH recombinations become weakly dependent on wavefunction overlap and their value remains constant. Correspondingly, the extrinsic droop process remains constant while the radiative rate is reduced – a trend which has been overlooked in previous studies focusing solely on radiative dynamics. We propose that this unfavorable balance of recombinations causes the green gap, and that improvements in long-wavelength III-Nitride emitters *at all currents* may be enabled by a reduction in SRH defects and the associated droop process.

* adavid@soraa.com

- [1] C. A. Hurni, A. David, M. J. Cich, R. I. Aldaz, B. Ellis, K. Huang, A. Tyagi, R. A. DeLille, M. D. Craven, and F. M. Steranka, *Applied Physics Letters* **106**, 031101 (2015).
- [2] Y. C. Shen, G. O. Mueller, S. Watanabe, N. F. Gardner, A. Munkholm, and M. R. Krames, *Applied Physics Letters* **91**, 141101 (2007).
- [3] A. David and M. J. Grundmann, *Applied Physics Letters* **96**, 103504 (2010).
- [4] J. Iveland, L. Martinelli, J. Peretti, J. S. Speck, and C. Weisbuch, *Physical Review Letters* **110**, 177406 (2013).
- [5] A. M. Armstrong, M. H. Crawford, and D. D. Koleske, *Applied Physics Express* **7**, 032101 (2014).
- [6] S. Hammersley, M. J. Kappers, F.-P. Massabuau, S. L. Sahonta, P. Dawson, R. A. Oliver, and C. J. Humphreys, *Applied Physics Letters* **107**, 132106 (2015).
- [7] S. Schulz, M. A. Caro, C. Coughlan, and E. P. O'Reilly, *Physical Review B* **91**, 035439 (2015).
- [8] M. Auf der Maur, A. Pecchia, G. Penazzi, W. Rodrigues, and A. Di Carlo, *Physical Review Letters* **116**, 027401 (2016).
- [9] F. Nippert, S. Y. Karpov, G. Callsen, B. Galler, T. Kure, C. Nenstiel, M. R. Wagner, M. Strassburg, H.-J. Lugauer, and A. Hoffmann, *Applied Physics Letters* **109**, 161103 (2016).
- [10] T. Akasaka, H. Gotoh, T. Saito, and T. Makimoto, *Applied physics letters* **85**, 3089 (2004).
- [11] C. Haller, J. F. Carlin, G. Jacopin, D. Martin, R. Butte, and N. Grandjean, *Applied Physics Letters* **111**, 262101 (2017).
- [12] C. Haller, J. F. Carlin, G. Jacopin, W. Liu, D. Martin, R. Butte, and N. Grandjean, *Applied Physics Letters* **113**, 111106 (2018).
- [13] T. Langer, A. Chernikov, D. Kalincev, M. Gerhard, H. Bremers, U. Rossow, M. Koch, and A. Hangleiter, *Applied Physics Letters* **103**, 202106 (2013).
- [14] A. David, N. G. Young, C. A. Hurni, and M. D. Craven, *Applied Physics Letters* **110**, 253504 (2017).
- [15] A. David, C. A. Hurni, N. G. Young, and M. D. Craven, *Applied Physics Letters* **109**, 033504 (2016).
- [16] G. Lasher and F. Stern, *Physical Review* **133**, A553 (1964).
- [17] A. David and M. J. Grundmann, *Applied Physics Letters* **97**, 033501 (2010).
- [18] C. M. Jones, C.-H. Teng, Q. Yan, P.-C. Ku, and E. Kioupakis, *Applied Physics Letters* **111**, 113501 (2017).
- [19] A. David, C. A. Hurni, N. G. Young, and M. D. Craven, *Applied Physics Letters* **111**, 233501 (2017).
- [20] This exponent is slightly different from the value $q = 1.3$ we found in Ref. [19]. This is because the former exponent was derived from a 1D Schrodinger model of I , whereas here we evaluate I empirically from $I \sim \sqrt{B}$.
- [21] More precisely, the first half of this layer is grown hot; the second half is grown at normal temperature, to ensure good morphology before growing the QW.
- [22] J. G. Fossum, R. P. Mertens, D. S. Lee, and J. F. Nijs, *Solid-state electronics* **26**, 569 (1983).
- [23] In this study, the high-In samples emit at long wavelength at low current (see Fig. 4) due to the strong QW polarization fields in our test structures. At higher current, the wavelength shifts to a more typical value due to field screening.
- [24] U. T. Schwarz, H. Braun, K. Kojima, Y. Kawakami, S. Nagahama, and T. Mukai, *Applied Physics Letters* **91** (2007).
- [25] A. David and N. F. Gardner, *Applied Physics Letters* **97**, 193508 (2010).